Journal of
Materials Chemistry C

Accepted Manuscript

This article can be cited before page numbers have been issued, to do this please use: J. Quinn, C. Guo, F. Haider, H. Patel, D. A. Khan and Y. Li, *J. Mater. Chem. C*, 2017, DOI: 10.1039/C7TC01204G.

ROYAL SOCIETY OF CHEMISTRY

rsc.li/materials-c

DOI: 10.1039/C7TC01204G

Journal Name

ARTICLE

Regioisomerism of alkyl-substituted bithiophene comonomer in (3*E*,8*E*)-3,8-bis(2-oxoindolin-3-ylidene)naphtho-[1,2-*b*:5,6-*b'*]difuran-2,7(3*H*,8*H*)-dione (INDF) based D-A polymers for organic thin film transistors

Received 00th January 20xx,
Accepted 00th January 20xx

DOI: 10.1039/x0xx00000x

www.rsc.org/

Jesse T. E. Quinn,‡ Chang Guo,‡ Fezza Haider, Haritosh Patel, Daid A. Khan and Yuning Li*

Two donor-acceptor (D-A) polymers based on (3*E*,8*E*)-3,8-bis(2-oxoindolin-3-ylidene)naphtha-[1,2-*b*:5,6-*b'*]difuran 2,7(3*H*,8*H*)-dione (INDF) and substituted regioisomeric bithiophene (BT) units with different side chain positions (head-to-head, HH, and tail-to-tail, TT) were synthesized. **PINDFBT-(HH)** achieved electron (μ_e) and hole (μ_h) mobilities as high as 0.33 $cm^2 V^{-1} s^{-1}$ and 0.15 $cm^2 V^{-1} s^{-1}$, respectively, while **PINDFBT-(TT)** showed a magnitude lower mobilities with μ_e of 0.07 $cm^2 V^{-1} s^{-1}$and μ_h of 0.02 $cm^2 V^{-1} s^{-1}$. The distinctly different electrical performance of these two polymers is originated from their different side chain placements on the bithiophene units and consequently differed electronic structures, backbone coplanarity, chain packing and thin film morphology. Our results showed that a bithiophene unit with an HH substitution pattern is much more favoured in terms of the charge transport property of the polymers.

Introduction

π-Conjugated polymers have attracted much attention as the semiconductor active layers in organic thin film transistors (OTFTs).[1-4] The favorable properties of polymer semiconductors such as printability, light weight, mechanical robustness, and tunable optoelectronic properties have made the polymer based OTFTs appealing for numerous applications such as the drivers for active-matrix flexible organic light-emitting diode (OLED) displays, logic circuits, phototransistors, and chemical and biological sensors. Extensive studies on OTFTs over the past several decades have gained deeper insight into the fundamental physics of π-conjugated organic semiconductors and new materials design[4-6] and led to considerable improvements in performance. In particular, the charge carrier mobility has surpassed 1 $cm^2 V^{-1} s^{-1}$ in both p- and n-channel OTFTs.[7-10]

Good solubility is a prerequisite for polymer semiconductors in order to fabricate OTFTs by printing techniques, which is essential for high throughput roll-to-roll manufacturing.[4] However, most polymers with only π-conjugated backbones are notorious for their poor solubility due to the high rigidity and strong intermolecular π-π interaction of backbones. A common strategy to render conjugated polymers soluble is to decorate the polymer backbone with flexible, often insulating, side chains. However, an excessive use (too many or too long) or inappropriate positioning of side chains would degrade the electrical performance of the polymers. Therefore, optimization of the side chain population, size, shape (e.g., straight or branched), as well as regioisomerism is needed to obtain sufficient solubility and yet to maintain optimal electrical performance of polymer semiconductors.[11-19]

Previously, our group reported a new electron accepting unit, (3*E*, 8*E*)-3,8-bis(2-oxoindolin-3-ylidene)naphtha-[1,2-*b*:5,6-*b'*]difuran 2,7(3*H*,8*H*)-dione (INDF).[20] INDF is an extension of the naphthodifuran (NDF) moiety, which polymers have showed modest hole mobilities in OTFTs.[21,22] When copolymerized with bithiophene (BT) a well-balanced ambipolar performance was achieved with high hole and electron mobilities of 0.51 and 0.50 $cm^2 V^{-1} s^{-1}$, respectively. Due to the large fused ring structure of INDF and the interchain D-A interaction, it was found that the PINDFBT polymer is poorly soluble in common solvents at room temperature even when two very large branched 4-octadecyldocosyl side chains were used on the INDF unit. A hot polymer solution was needed for spin coating in order to obtain a good film. To address this solubility issue, in this study, we introduced an additional alkyl (dodecyl) side chain on each of thiophenes in the bithiophene unit while cutting down the size of the alkyl side chains on the INDF unit to the smaller 2-decyltetradecyl groups. The two dodecyl side chains on the bithiophene unit are positioned in two manners: tail-to-tail (TT) and head-to-head (HH), resulting in two polymers

*Department of Chemical Engineering and Waterloo Institute for Nanotechnology (WIN), University of Waterloo, 200 University Ave West, Waterloo, Ontario, N2L 3G1, Canada. *E-mail: yuning.li@uwaterloo.ca; Fax: +1 519-888-4347; Tel: +1 519-888-4567 ext. 31105*

†Electronic Supplementary Information (ESI) available: [details of any supplementary information available should be included here]. See DOI: 10.1039/x0xx00000x

‡ These two authors made equal contributions.

View Article Online
DOI: 10.1039/C7TC01204G

PINDFBT-(TT) and **PINDFBT-(HH)** (Scheme 1). These two polymers showed much improved solubility in common solvents although the overall size of the alkyl substituents in every repeat unit is reduced compared to the 4-octadecyldocosyl (C40) substituted polymer **PINDFBT-40**. However, the alkyl side chain arrangement (TT or HH), i.e., the regioisomerism, of the bithiophene units was found to have profound impacts on the properties including the charge transport performance in OTFTs of **PINDFBT-(TT)** and **PINDFBT-(HH)**.

Results and discussion

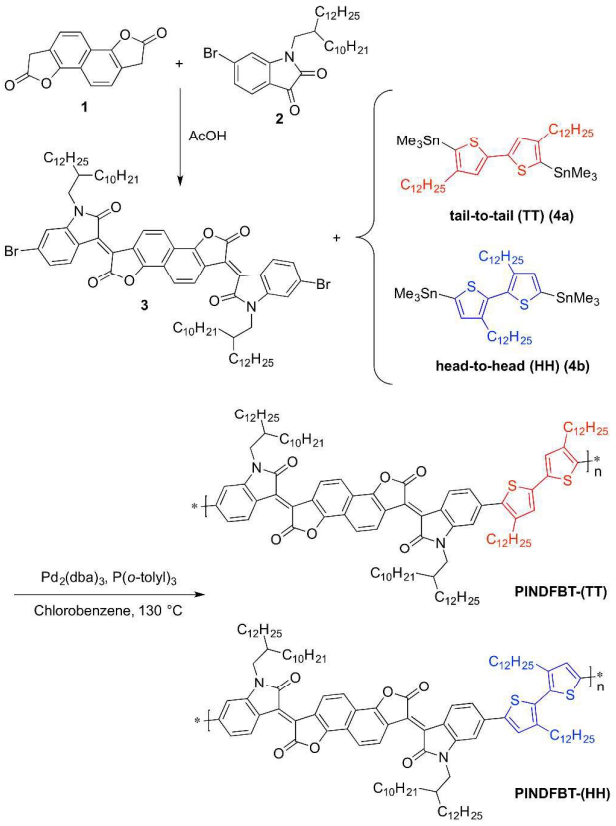

Scheme 1 Synthetic route to **PINDFBT(TT)** and **PINDFBT(HH)**.

Scheme 1 illustrates the synthetic route to the two regioisomeric INDF-based polymers, **PINDFBT-(TT)** and **PINDFBT-(HH)**. The 2-decyltetradecyl substituted INDF dibromo monomer **3** was prepared from 6-bromo-1-(2-decyltetradecyl)indoline-2,3-dione (**1**) and 1,6-dihydronaphtho[1,2-*b*:5,6-*b'*]difuran-2,7-dione (**2**) following the procedure reported previously.[23] The two dodecyl substituted bithiophene-based regioisomeric ditin compounds **4a** and **4b** with the TT and HH side chain arrangements, respectively, were prepared according to literature.[24,25] **3** was reacted with either **4a** or **4b** under a typical Stille coupling polymerization condition using Pd_2dba_3/P(*o*-tolyl)$_3$ as the catalyst and chlorobenzene as the solvent, forming **PINDFBT-(TT)** and **PINDFBT-(HH)**, respectively. After Soxhlet extraction

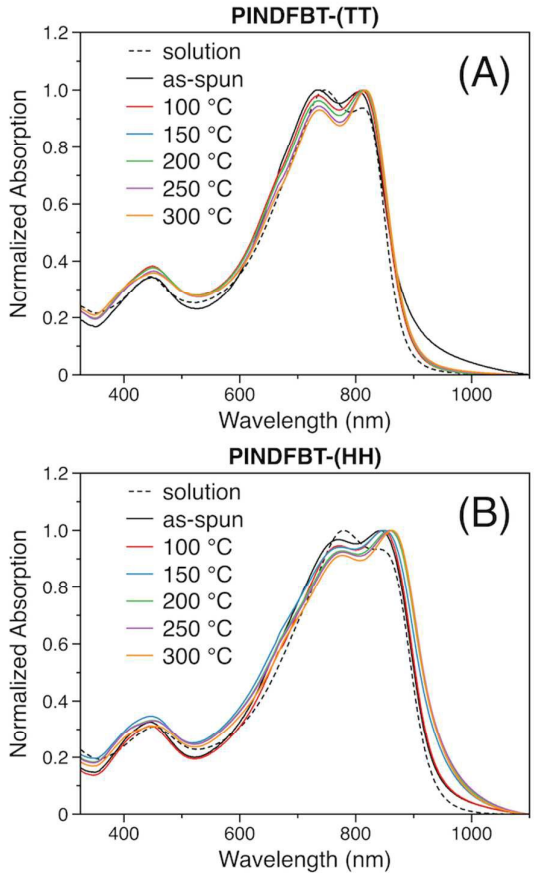

Fig. 1 The UV-Vis-NIR absorption spectra of **PINDFBT-(TT)** (A) and **PINDFBT-(HH)** (B) in chloroform solutions and as thin films (as-spun and annealed at different temperatures).

purification with acetone, hexanes, and chloroform successively, **PINDFBT-(TT)** and **PINDFBT-(HH)** were obtained in high yields of 91% and 96%, respectively. Both polymers showed much improved solubility in some common solvents such as chloroform, chlorobenzene, 1,2-dichlorobenzene, tetrachloroethane, and toluene at room temperature in comparison with **PIBDFBT-40**. The molecular weights of the polymers were characterized by high temperature gel permeation chromatography (HT-GPC) at 140 °C using 1,2,4-tricholorobenzene as the eluent and polystyrene as standards. The number average molecular weight (M_n) and polydispersity index (PDI) are 19.4 kDa and 3.5 for **PINDFBT-(TT)** and 25.8 kDa and 3.0 for **PINDFBT-(HH)**. Both polymers showed high thermal stability with 5% weight loss temperatures ($T_{-5\%}$) at 376 and 380 °C for **PINDFBT-(TT)** and **PINDFBT-(HH)**, respectively, as revealed by thermal gravimetric analysis (TGA, ESI†). No noticeable endo- or exothermic transitions were observed on their differential scanning calorimetry (DSC) thermograms up to 340 °C (ESI†), indicating that both polymers have very high melting points (both polymers are crystalline, which were confirmed by the XRD measurement as discussed below).

Fig. 1 shows the UV-Vis-NIR absorption spectra of the two polymers in chloroform solutions and as thin films (as-spun

View Article Online
DOI: 10.1039/C7TC01204G

Table 1 Photophysical and electrochemical properties of **PINDFBT-(TT)** and **PINDFBT-(HH)**.

Polymer	λ_{max} (nm)		E_g^{opt} (eV)	HOMO (eV)	LUMO (eV)	E_g^{ec} (eV)
	Solution	Film (as-spun)				
PINDFBT-(TT)	447, 747, 812 (s)[a]	446, 737, 804 (s)	1.39	-5.76	-3.78	1.98
PINDFBT-(HH)	452, 779, 844 (s)	445, 767 (s), 845	1.31	-5.68	-3.77	1.91

[a] Shoulder

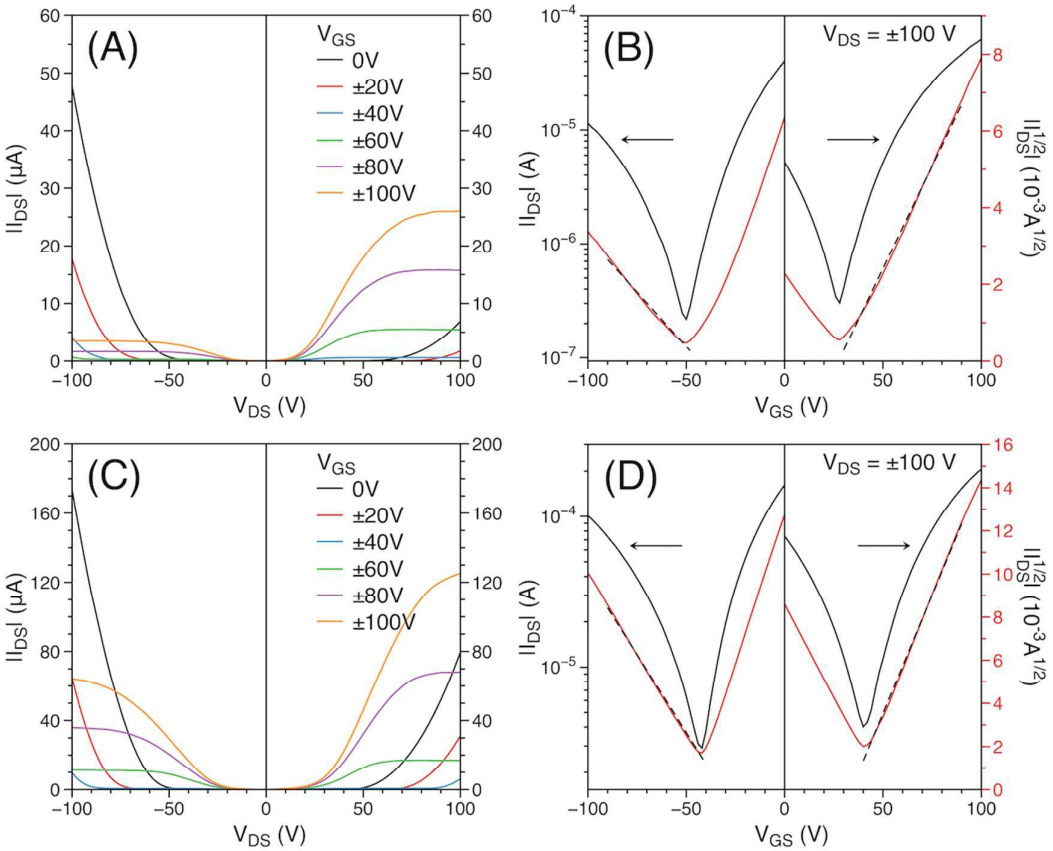

Fig. 2 Transfer (right) and output (left) curves of OTFT **PINDFBT-TT** (A and B) and **PINDFBT-HH** (C and D) based BGBC OTFT devices. The polymer thin films were annealed at 250 °C. Device dimensions: channel width (W) = 30 μm; channel length (L) = 1000 μm.

and annealed at different temperatures). Dual band absorption was observed, which is typical for D–A π-conjugated systems with the lower energy band originated from the intramolecular charge transfer (ICT) from the donor unit (bithiophene) to the acceptor unit (INDF) and the higher energy band originated from the π-π* transition. The lower energy band of each polymer further showed two distinct peaks, representing vibronic splitting. The maximum absorption wavelengths (λ_{max}) for **PINDFBT-(TT)** and **PINDFBT-(HH)** in solutions are 747 nm and 779 nm (Table 1), respectively. A hypsochromic shift of ~10 nm from solution to solid state was observed for **PINDFBT-(TT)**, which is characteristic of H-aggregation.[26,27] For **PINDFBT-(HH),** the vibronic splitting transition low energy shoulder at 845 nm became the strongest absorption peak, suggesting **PINDFBT-(HH)** formed more ordered chain packing compared to **PINDFBT-(TT)**. With increasing annealing temperature from 50 °C to 300 °C, both polymers showed bathochromic shifts with intensified low-energy vibronic bands in their absorption profiles, indicating their increasing chain ordering. The optical band-gaps (E_g^{opt}) calculated from the onset absorption wavelengths of the as-spun thin film spectra are 1.39 and 1.31 eV for **PINDFBT-(TT)** and **PINDFBT-(HH)**, respectively. As will be discussed in more detail later, the computational simulations showed that the incorporation of dodecyl side chains on the bithiophene unit, either TT or HH, caused severe polymer backbone twisting. For **PINDFBT-(TT)**, the major twisting occurs at the junction between INDF and thiophene, primarily caused by the dodecyl side chain. On the other hand, for **PINDFBT-(HH)**, the most twisted position is located at the linkage between two thiophenes. For a D-A polymer, the band gap is mainly governed by the HOMO energy of the donor unit and the LUMO energy of the acceptor unit through the ICT process. Evidently, the twisting at the junction between the INDF (acceptor) and thiophene (donor) in **PINDFBT-(TT)** would disrupt the ICT resulting in a larger band gap compared to **PINDFBT-(HH)**, in which the junction between the INDF and thiophene is relatively coplanar providing a much more efficient ICT process and thus a smaller band gap.

View Article Online
DOI: 10.1039/C7TC01204G

Cyclic voltammetry (CV) measurements were performed on polymer thin films to estimate the frontier orbital energy levels of the polymers (Table 1 and ESI†). By using the oxidative onset potentials, the HOMO energy levels were calculated to be -5.76 and -5.68 eV for **PINDFBT-(TT)** and **PINDFBT-(HH)**, respectively. The LUMO energy levels were calculated from the reduction onset potentials to be -3.78 eV and -3.77 eV for **PINDFBT-(TT)** and **PINDFBT-(HH)**, respectively. These results indicate that the different arrangements of side chains on the thiophene units had little influence on the LUMO energy levels, but a large effect on their HOMO energy levels. The severe backbone twisting, which comes from the side chain steric effect between INDF and thiophenes units, in **PINDFBT-(TT)** might have disrupted the HOMO hybridization between these two units, resulting in a lower HOMO energy level. On the other hand, the LUMO energy level is mainly determined by the acceptor INDF unit and thus less affected by the twisting occurred at the INDF-thiophene junction. The electrochemical band gaps (E_g^{ec}) calculated from the CV results are 1.98 eV for **PINDFBT-(TT)** and 1.91 eV for **PINDFBT-(HH)**. The differences between the bandgaps measured by CV and UV-Vis-NIR, which represent the exciton binding energies, are 0.59 eV for **PINDFBT-(TT)** and 0.60 eV for **PINDFBT-(HH)**, which are in the typical range (0.3-1 eV) for π-conjugated polymers.[28]

The charge transport performance of the polymers was evaluated by using them as channel layers in bottom-gate bottom-contact (BGBC) OTFT devices, where n^{++}-doped silicon wafer with a 300 nm thermally grown SiO_2 layer was used as substrate. The gold source and drain electrodes were pre-patterned and the SiO_2 surface was modified with dodecyltrichlorosilane (DDTS) to ensure minimal surface charge traps. The channel layer was formed by spin coating a polymer solution (5 mg mL^{-1}) onto the substrate. The fabrication and characterization of the OTFT devices were carried out in a nitrogen-filled glove box. Both polymers showed electron charge transport dominant field effect transistor characteristics (Fig. 3). For devices based on **PINDFBT-(TT)**, the best overall performance with an electron mobility (μ_e) of 7.17×10^{-2} cm^2 V^{-1} s^{-1} and hole mobility (μ_h) of 2.17×10^{-2} cm^2 V^{-1} s^{-1} was achieved for the films annealed at 250 °C. After annealing at a higher temperature of 300 °C, the μ_h showed slight improvement, whereas the μ_e showed a significant decline. The devices based on **PINDFBT-(HH)** displayed significantly better performance. The highest μ_e and μ_h of 0.33 cm^2 V^{-1} s^{-1} and 0.15 cm^2 V^{-1} s^{-1}, respectively, were achieved for the films annealed at 250 °C. The electron and hole mobilities of **PINDFBT-(TT)** and **PINDFBT-(HH)** are lower than those (up to 0.51 cm^2 V^{-1} s^{-1} and 0.50 cm^2 V^{-1} s^{-1}, respectively)[20] of **PINDFBT-40** that has no side chain substitution on the bithiophene unit. The lower mobilities of **PINDFBT-(TT)** and **PINDFBT-(HH)** can be explained by the severe twisting of their polymer backbones caused by the introduction of dodecyl side chains on the bithiophene unit, which would interrupt the intramolecular chain transport. However, the mobilities of **PINDFBT-(TT)** dropped much more significantly, while the mobilities of **PINDFBT-(HH)** are fairly maintained compared to those of **PINDFBT-40**. Particularly,

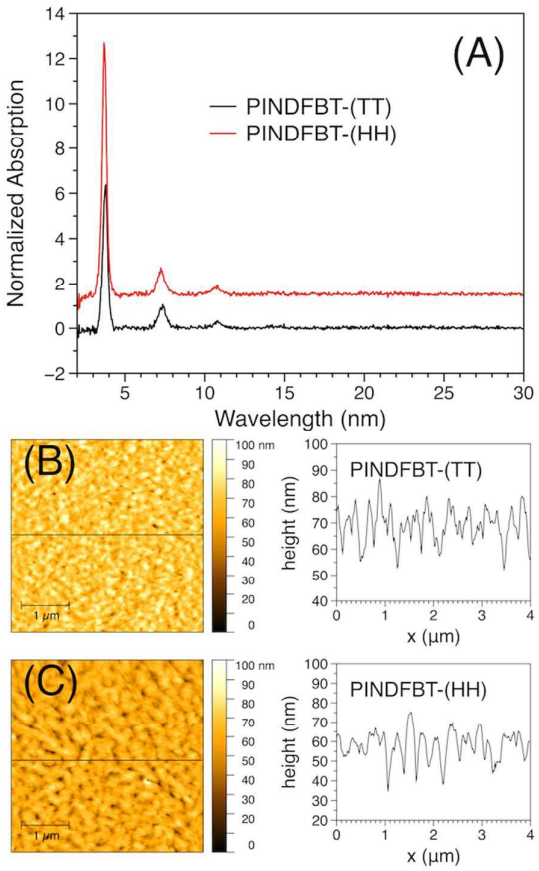

Fig. 3 (A) XRD of polymer thin films annealed at 250 °C. (B) and (C) AFM height images and profiles of **PINDFBT-(TT)** and **PINDBT-(HH)** annealed at 250 °C with a scan area of 4 μm × 4 μm. The root mean square roughness (R_q) is ~ 6 nm and ~7 nm for **PINDFBT-(TT)** and **PINDFBT-(HH)**, respectively.

the average electron mobilities of **PINDFBT-(HH)** is 0.21-0.31 cm^2 V^{-1} s^{-1} (ESI†), which are comparable to the average electron mobilities of 0.17-0.37 cm^2 V^{-1} s^{-1} obtained for **PINDFBT-40**.[20] It is also noticed that the variations in the mobilities are much smaller for **PINDFBT-(HH)** (~8-14%) than for **PINDFBT-40** (~15-31%) owing to the much improved solubility and thus film quality of the former. It should be noted that both **PINDFBT-(TT)** and **PINDFBT-(HH)** displayed electron transport dominant ambipolar charge transport behavior with a μ_e/μ_h ratio of ~2-3, while **PINDFBT-40** showed a quite balanced μ_e/μ_h ratio of close to 1. The relatively low hole mobilities observed for **PINDFBT-(TT)** and **PINDFBT-(HH)** may be due to the interrupted HOMO pathways, which are mainly localized around the bithiophene units (see the computer simulation results shown in Fig. 4).

X-ray diffraction (XRD) was employed to investigate the crystallinity and thus the chain ordering of the polymer thin films annealed at 250 °C, which offered the optimal OTFT performance. As shown in Fig. 3, the thin films of both polymers are quite crystalline. Diffraction peaks up to the third order are clearly observed at 2θ = 3.80° (100), 7.37° (200), and 10.81° (300) for **PINDFBT-(TT)** and at 2θ = 3.68° (100), 7.25° (200), and 10.77° (300) for **PINDFBT-(HH)**. The corresponding

View Article Online
DOI: 10.1039/C7TC01204G

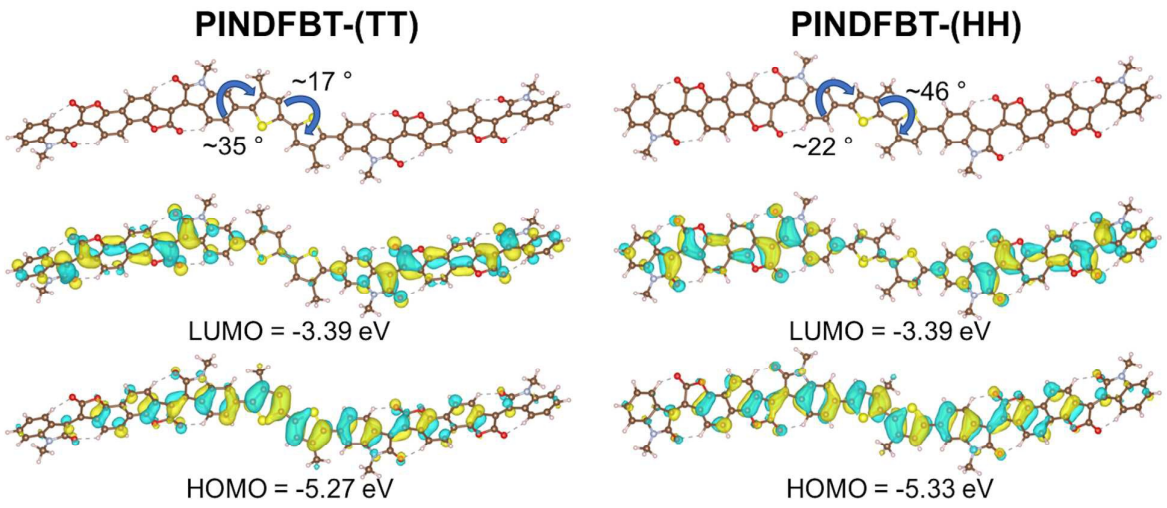

Fig. 4 The optimized ground state structures and wavefunctions for the frontier molecular orbitals of the projected models of **PINDFBT-(TT)** and **PINDFBT-(HH)**, respectively, obtained by DFT calculations at the B3LYP/6-31G(d) level of theory.

d-spacing distances are 2.32 nm for **PINDFBT-(TT)** and 2.40 nm for **PINDFBT-(HH)**. An edge-on orientation motif relative to the substrate was believed to be adopted as there is no noticeable interchain π-π stacking reflection peaks that should appear around 2θ = ~20–25°.[29,30] The diffraction intensity observed for **PINDFBT-(TT)** is weaker compared to **PINDFBT-(HH)** indicating that the former formed less ordered chain packing, which is another factor that leads to its poorer charge transport performance in OTFTs.

The morphological properties of the 250 °C-annealed polymer films were examined by atomic force microscopy (AFM) and the height images are shown in Fig. 3. Both polymer films exhibited clear domain aggregates with similar roughness (with the root mean square roughness (R_q) of ~6 nm and ~7 nm for **PINDFBT-(TT)** and **PINDFBT-(HH)**, respectively). However, **PINDFBT-(HH)** showed much large aggregates, which is likely due to its higher crystallinity than that of **PINDFBT-(TT)** verified by the XRD measurements.

We studied the optimized geometry and electronic structure of these alkylated bithiophene polymers using a quantum chemistry approach.[31] To reduce computational time, an acceptor-donor-acceptor (A-D-A) structure of the respective polymers were used along with methyl substituents as proxies of the alkyl side chains (Fig. 4). Geometries were optimized at the B3LYP/6-31G(d) level and the nature of the minima was confirmed by the eigenvalues (all positive) of the corresponding Hessian matrices. The calculations revealed that the projected model of **PINDFBT-(TT)** is quite twisted between the INDF moiety and the adjacent thiophene unit with a dihedral angle of ~35 °, whereas the projected model of **PINDFBT-(HH)** has a smaller dihedral angle of ~22 ° at this junction. The root cause of the large twisting between INDF and thiophene in **PINDFBT-(TT)** is due to the repulsion between the methyl sidechain and the neighboring hydrogen atom on the benzene ring. The dihedral angles between the thiophene units are ~17 ° and ~46 ° for **PINDFBT-(TT)** and **INDFBT-(HH)**, respectively. The much larger dihedral angle for **PINDFBT-(HH)** is caused by the repulsion between the methyl side chain and the sulfur atom of the neighboring thiophene. Compared with **PINDFBT-40**, which has a dihedral angle of ~20° between INDF and thiophene and ~14° between the two thiophene units, **PINDFBT-(TT)** has a much less coplanar backbone with notably increased twisting at the thiophene-thiophene junction. A highly coplanar backbone has been generally considered favorable for charge carrier transport because of the more extended π-electron delocalization. While the reduced coplanarity might explain the observed low mobilities of **PINDFBT-(TT)**, it does not apply to **PINDFBT-(HH)**, which also has a quite twisted backbone, but showed comparable mobilities to those of **PINDFBT-40**. Recently, a few polymers have demonstrated high mobilities despite of their highly twisted backbone,[32,33] which was explained by the reduced degrees of backbone rotational freedom, leading to higher degrees of ordering (or crystallinity).[33] In our case, **PINDFBT-(HH)** showed higher crystallinity than **PINDFBT-(TT)**, which indicates that **PINDFBT-(HH)** may have a smaller degree of rotational freedom, leading to its high mobility. The LUMO energy level was calculated to be -3.39 eV for both model compounds while **PINDFBT-(TT)** had a slightly higher HOMO energy level of -5.27 eV as opposed to -5.33 eV for **PINDFBT-(HH)**. The wavefunction of the LUMO energy level appears to be localized within the INDF moieties whereas the wavefunction of the HOMO energy level appears to be distributed more preferably at the bithiophene and its adjacent part of the neighboring INDF moieties for both projected model compounds. The calculated LUMO energy levels agree with the experimental trend (see discussions on the CV data above). However, the calculated HOMO energy levels show an opposite trend compared to what is observed experimentally. This discrepancy may be explained by the intermolecular interaction of the actual polymer chains, which was not taken into account in the optimization and hessian calculations. The backbone coplanarity of these two polymers may also change dramatically and differently in the solid state.

View Article Online
DOI: 10.1039/C7TC01204G

Experimental

Materials and characterization

Starting materials and reagents were purchased from commercial sources and used without further purification. 6-Bromo-1-(2-decyltetradecyl)indoline-2,3-dione (**1**),[23] 1,6-dihydronaphtho[1,2-*b*:5,6-*b'*]difuran-2,7-dione (**2**)[20] (4,4'-Didodecyl-[2,2'-bithiophene]-5,5'-diyl)bis(trimethylstannane) (**4a**)[24] and (3,3'-didodecyl-[2,2'-bithiophene]-5,5'-diyl)bis(trimethylstannane) (**4b**)[25] were prepared according to the literature methods. NMR data were recorded on a Bruker DPX 300 MHz spectrometer with chemical shifts relative to the residual $CHCl_3$ in the deuterated solvent (7.26 ppm for $CHCl_3$).[34] The mass spectra (MALDI-TOF) was recorded on a Bruker Autoflex Speed MALDI-TOF mass spectrometer. The UV-Vis-NIR absorption spectra of polymers were recorded on a Thermo Scientific GENESYS^{TM} 10S VIS spectrophotometer. CV data were obtained on a CHI600E electrochemical analyser using an Ag/AgCl reference electrode and two Pt disk electrodes as the working and counter electrodes in a 0.1 M tetrabutylammonium hexafluorophosphate solution in anhydrous acetonitrile at a scan rate of 50 mV s^{-1}. Ferrocene was used as the reference, which has a HOMO energy level of -4.8 eV.[35] AFM images were taken on polymer thin films spin coated on dodecyltrichlorosilane modified SiO_2/Si substrates and annealed at 250 °C for 15 min in nitrogen using a Dimension 3100 scanning probe microscope. Reflection mode XRD diagrams of polymer thin films (~40 nm) spin coated on dodecyltrichlorosilane-modified SiO_2/Si substrates and annealed at 250 °C for 15 min in nitrogen were obtained using a Bruker D8 Advance powder diffractometer with Cu Ka radiation (λ = 0.15406 nm). Density functional theory (DFT) through Gaussian 09 Revision D.01[31] using the functional B3LYP and the basis set 6-31G(d) or 6-31G(d,p) under tight convergence to investigate the geometry, molecular energy levels, and electron distributions for model compounds. GPC measurements of polymers were performed on a Malvern HT-GPC using 1,2,4-trichlorobenzene as an eluent and polystyrene as standards at 140 °C. TGA measurements were carried out on a TA Instruments Q500 at a temperature ramping rate of 10 °C min^{-1} under nitrogen. DSC measurements were carried out on a TA Instruments Q2000 at a temperature ramping rate of 20 °C min^{-1} under nitrogen.

Synthesis of 1,6-bis((*E*)-6-bromo-1-(2-decyltetradecyl)-2-oxoindolin-3-ylidene)-1,6-dihydronaphtho[1,2-*b*:5,6-*b'*]difuran-2,7-dione (3)

To a 100 mL flask, **2** (0.38 g, 1.6 mmol), **1** (1.62 g, 3.2 mmol) and *p*-toluenesulfonic acid (77.1 mg, 0.45 mmol) were added. Then the flask was evacuated and purged with nitrogen three times before acetic acid (30 mL) was added. The reaction mixture was stirred at 115 °C for 24 h, cooled down to room temperature, and filtered. The collected solid was washed with methanol. The crude product was then purified by silica gel column chromatography at 50 °C using a mixture of heptane and chloroform (1:1) as eluent to afford a brown solid as the title product (0.39 g, 20 %). ^{1}H NMR (300 MHz, $CDCl_3$) δ 9.16 (d, *J* = 9.1 Hz, 2H), 8.88 (d, *J* = 8.6 Hz, 2H), 7.78 (d, *J* = 9.1 Hz, 2H), 7.20 (d, *J* = 8.7 Hz, 2H), 6.86 (s, 2H), 3.60 (d, *J* = 7.4 Hz, 4H), 1.88 (br, 2H), 1.25 (m, 80H), 0.87 (t, *J* = 6.4 Hz, 12H). ^{13}C NMR (100 MHz, $CDCl_3$) δ 166.64, 146.99, 131.07, 128.36, 126.63, 121.50, 120.04, 117.81, 111.97, 36.24, 32.08, 31.71, 30.16, 29.82, 29.78, 29.51, 26.55, 22.84, 14.27. MS (MALDI-TOF) *m/z*: 1329.7 $(M+H)^+$.

PINDFBT-(TT)

To a 25 mL dry Schlenk flask, **3** (0.15 g, 0.12 mmol), **4a** (0.10 g, 0.12 mmol), and tri(*o*-tolyl)phosphine (P(*o*-tolyl)$_3$) (2.9 mg, 0.010 mmol) were charged. After degassing and refilling argon for three times, anhydrous chlorobenzene (3 mL) and tris(dibenzylideneacetone)-dipalladium ($Pd_2(dba)_3$) (2.2 mg, 0.002 mmol) were added. The reaction mixture was stirred at 130 °C for 60 h. Upon cooling to room temperature, the reaction mixture was poured into stirring methanol (100 mL). The precipitate was collected by filtration and subject to Soxhlet extraction with acetone, hexanes, and chloroform successively. Drying the chloroform extract gave 175 mg (91.4 %) of **PINDFBT-(TT)**.

PINDFBT-(HH)

This polymer was synthesized following a similar procedure used for the preparation of **PINDFBT-(TT)**, except of using **4b** instead of **4a**. After Soxhlet extraction purification and removal of solvent from the chloroform extract, 183 mg (95.5 %) of **PINDFBT-(HH)** was obtained.

Fabrication and characterization of organic thin film transistors (OTFTs)

A bottom-gate bottom-contact (BGBC) configuration was used for all OTFT devices. The device fabrication procedure is as follows. A heavily n^{++}-doped SiO_2/Si wafer with ~300 nm-thick SiO_2 was patterned with gold source and drain pairs by conventional photolithography and thermal deposition techniques. Subsequently, the substrate was treated with O_2-plasma, followed by cleaning with acetone and then isopropanol in an ultrasonicating bath. Then the substrate was placed in a solution of dodecyltrichlorosilane in toluene (10 mg mL^{-1}) at room temperature for 20 min, followed by washing with toluene and drying under a nitrogen flow. A polymer solution in chloroform (5 mg mL^{-1}) was spin coated onto the substrate at 3000 rpm for 60 s to give a polymer film (~40 nm), which was subject to thermal annealing at a select temperature for 20 min in a glove box. All the OTFT devices have a channel length (*L*) of 30 μm and a channel width (*W*) of 1000 μm. Devices were characterized in the same glove box using an Agilent B2912A Precision Source/Measure Unit. The reported mobility (μ) values were calculated using the saturated regime current–voltage characteristics represented with the drain–source current (I_{DS}) equation:

$$I_{DS} = \left(\frac{WC_i}{2L}\right)\mu(V_G - V_{th})^2$$

View Article Online
DOI: 10.1039/C7TC01204G

where C_i is the capacitance per unit area of the dielectric (11.6 nF cm^{-2}), W (1000 μm) and L (30 μm) are OTFT channel width and length, V_G is the gate voltage, and V_{th} is the threshold voltage.

Conclusions

Two new polymers based on 2-decylteradecyl substituted (3*E*, 8*E*)-3,8-bis(2-oxoindolin-3-ylidene)naphtha-[1,2-*b*:5,6-*b'*]difuran 2,7(3*H*,8*H*)-dione (INDF) and dodecyl substituted regioisomeric BT units, **PINDFBT-(HH)** and **PINDFBT-(TT)**, were synthesized and characterized. These polymers showed much improved solubility than the previously reported polymer **PINDFBT-40** having 4-octadecyldocosyl substituted INDF units and non-substituted bithiophene units. It was found that **PINDFBT-(TT)** showed a larger band gap and a lower degree of crystallinity compared to **PINDFBT-(HH)**, caused by the severe twisting at the junction between INDF and the 4-dodecylthiophene unit. **PINDFBT-(HH)**, which has higher coplanarity at the INDF and thiophene junction, but a more twisted junction between the two 3-dodecylthiopehne units. In OTFTs, **PINDFBT-(HH)** achieved high ambipolar charge transport performance with electron and hole mobilities of up to 0.33 cm^2 V^{-1} s^{-1} and 0.15 cm^2 V^{-1} s^{-1}, respectively. The average electron mobilities of OTFTs based on **PINDFBT-(HH)** (0.21-0.31 cm^2 V^{-1} s^{-1}) are comparable to those of **PINDFBT-40** (0.17-0.37 cm^2 V^{-1} s^{-1}), but the former showed much smaller variations due to the improved solubility and thus film quality of **PINDFBT-(HH)**. On the other hand, **PINDFBT-(TT)** showed one order of magnitude lower electron and hole mobilities (up to 0.07 cm^2 V^{-1} s^{-1}and 0.02 cm^2 V^{-1} s^{-1}, respectively) caused by the severe twisting at the junction between INDF and bithiophene, which disrupted the intramolecular charge transfer and the backbone π-conjugation as well as polymer chain packing. This study demonstrated that the regioisomerism of the bithiophene comonomer unit have profound impacts on the optoelectronic properties, molecular packing as well as charge transport performance of the polymers. Our results show that a bithiophene unit with a head-to-head substitution pattern is able to minimize the negative impact of backbone twisting on the electron transport performance of the resulting polymer in comparison with the bithiophene unit with a tail-to-tail structure.

Acknowledgements

YL thanks the financial support of this work by the Natural Sciences and Engineering Research Council (NSERC) of Canada (Discovery Grant # RGPIN-2016-04366).

Notes and references

1 G. H. Gelinck, H. E. A. Huitema, E. van Veenendaal, E. Cantatore, L. Schrijnemakers, J. B. P. H. van der Putten, T. C. T. Geuns, M. Beenhakkers, J. B. Giesbers, B.-H. Huisman, E. J. Meijer, E. M. Benito, F. J. Touwslager, A. W. Marsman, B. J. E. van Rens and D. M. de Leeuw, *Nat Mater*, 2004, **3**, 106–110.
2 G. Gelinck, P. Heremans, K. Nomoto and T. D. Anthopoulos, *Adv. Mater.*, 2010, **22**, 3778–3798.
3 L. Torsi, M. Magliulo, K. Manoli and G. Palazzo, *Chem. Soc. Rev.*, 2013, **42**, 8612–8617.
4 H. Sirringhaus, *Adv. Mater.*, 2014, **26**, 1319–1335.
5 H. Klauk, *Chem. Soc. Rev.*, 2010, **39**, 2643–2666.
6 C. Wang, H. Dong, W. Hu, Y. Liu and D. Zhu, *Chem. Rev.*, 2012, **112**, 2208–2267.
7 G. Kim, S. J. Kang, G. K. Dutta, Y.-K. Han, T. J. Shin, Y.-Y. Noh and C. Yang, *J. Am. Chem. Soc.*, 2014, **136**, 9477–9483.
8 B. Sun, W. Hong, Z. Yan, H. Aziz and Y. Li, *Adv. Mater.*, 2014, **26**, 2636–2642.
9 R. Matsidik, H. Komber, A. Luzio, M. Caironi and M. Sommer, *J. Am. Chem. Soc.*, 2015, **137**, 6705–6711.
10 B. Nketia-Yawson, H.-S. Lee, D. Seo, Y. Yoon, W.-T. Park, K. Kwak, H. J. Son, B. Kim and Y.-Y. Noh, *Adv. Mater.*, 2015, **27**, 3045–3052.
11 J. Mei and Z. Bao, *Chem. Mater.*, 2014, **26**, 604–615.
12 C. B. Nielsen, R. S. Ashraf, S. Rossbauer, T. Anthopoulos and I. McCulloch, *Macromolecules*, 2013, **46**, 7727–7732.
13 B. Fu, J. Baltazar, A. R. Sankar, P.-H. Chu, S. Zhang, D. M. Collard and E. Reichmanis, *Adv. Funct. Mater.*, 2014, **24**, 3734–3744.
14 G. Zhang, P. Li, L. Tang, J. Ma, X. Wang, H. Lu, B. Kang, K. Cho and L. Qiu, *Chem. Commun.*, 2014, **50**, 3180–3183.
15 D. Gao, K. Tian, W. Zhang, J. Huang, Z. Chen, Z. Mao and G. Yu, 2016, **7**, 4046–4053.
16 X. Wang, H. H. Choi, G. Zhang, Y. Ding, H. Lu, K. Cho and L. Qiu, *J. Mater. Chem. C*, 2016, **4**, 6391–6400.
17 X.-Y. Wang, M.-W. Zhang, F.-D. Zhuang, J.-Y. Wang and J. Pei, *Polym. Chem.*, 2016, **7**, 2264–2271.
18 T. Hasegawa, M. Ashizawa, J. Hiyoshi, S. Kawauchi, J. Mei, Z. Bao and H. Matsumoto, *Polymer Chemistry*, 2016, **7**, 1181–1190.
19 H. Sirringhaus, P. J. Brown, R. H. Friend, M. M. Nielsen, K. Bechgaard, B. M. W. Langeveld-Voss, A. J. H. Spiering, R. A. J. Janssen, E. W. Meijer, P. Herwig and D. M. de Leeuw, *Nature*, 1999, **401**, 685–688.
20 Y. Deng, B. Sun, Y. He, J. Quinn, C. Guo and Y. Li, *Chem. Commun.*, 2015, **51**, 13515–13518.
21 S. Shi, K. Shi, S. Chen, R. Qu, L. Wang, M. Wang, G. Yu, X. Li and H. Wang, *J. Polym. Sci. Part A: Polym. Chem.*, 2014, **52**, 2465–2476.
22 S. Shi, K. Shi, G. Yu, X. Li and H. Wang, *RSC Advances*, 2015, **5**, 70319–70322.
23 Z. Yan, B. Sun and Y. Li, *Chem. Commun.*, 2013, **49**, 3790–3792.
24 W. Yue, Y. Zhao, H. Tian, D. Song, Z. Xie, D. Yan, Y. Geng and F. Wang, *Macromolecules*, 2009, **42**, 6510–6518.
25 B. Fu, J. Baltazar, Z. Hu, A.-T. Chien, S. Kumar, C. L. Henderson, D. M. Collard and E. Reichmanis, *Chem. Mater.*, 2012, **24**, 4123–4133.
26 H. Hwang, D. Khim, J.-M. Yun, E. Jung, S.-Y. Jang, Y. H. Jang, Y.-Y. Noh and D.-Y. Kim, *Adv. Funct. Mater.*, 2015, **25**, 1146–1156.
27 X. Zhang, J. P. Johnson, J. W. Kampf and A. J. Matzger, *Chem. Mater.*, 2006, **18**, 3470–3476.
28 E. Conwell, in *Primary Photoexcitations in Conjugated Polymers: Molecular Exciton Versus Semiconductor Band Model*, WORLD SCIENTIFIC, 1998, pp. 99–114.

View Article Online
DOI: 10.1039/C7TC01204G

29 B. Manoj and A. G. Kunjomana, *Int J Electrochem Sci*, 2012, **7**, 3127–3134.
30 Y. Hishiyama and M. Nakamura, *Carbon*, 1995, **33**, 1399–1403.
31 M. J. Frisch, G. W. Trucks, H. B. Schlegel and G. E. Scuseria, *Gaussian 09, revision D. 01*, 2009.
32 B. Kang, R. Kim, S. B. Lee, S.-K. Kwon, Y.-H. Kim and K. Cho, *J. Am. Chem. Soc.*, 2016, **138**, 3679–3686.
33 K. J. Fallon, N. Wijeyasinghe, E. F. Manley, S. D. Dimitrov, S. A. Yousaf, R. S. Ashraf, W. Duffy, A. A. Y. Guilbert, D. M. E. Freeman, M. Al-Hashimi, J. Nelson, J. R. Durrant, L. X. Chen, I. McCulloch, T. J. Marks, T. M. Clarke, T. D. Anthopoulos and H. Bronstein, *Chem. Mater.*, 2016, **28**, 8366–8378.
34 H. E. Gottlieb, V. Kotlyar and A. Nudelman, *J. Org. Chem.*, 1997, **62**, 7512–7515.
35 J. Pommerehne, H. Vestweber, W. Guss, R. F. Mahrt, H. Bässler, M. Porsch and J. Daub, *Adv. Mater.*, 1995, **7**, 551–554.

View Article Online
DOI: 10.1039/C7TC01204G

Graphical abstract

Two polymers based on (3*E*,8*E*)-3,8-bis(2-oxoindolin-3-ylidene)naphtha-[1,2-*b*:5,6-*b'*]difuran 2,7(3*H*,8*H*)-dione (INDF) and substituted regioisomeric bithiophene units show distinctly different charge transport performance.